ChemComm

COMMUNICATION

View Article Online
View Journal

Cite this: DOI: 10.1039/d6cc00483k

Received 23rd January 2026,
Accepted 4th March 2026

DOI: 10.1039/d6cc00483k

rsc.li/chemcomm

Visible-light-driven photoreductive complete degradation of sulfur hexafluoride under ambient conditions

Hu Zhang,[a] Yi-Ming Chen,[a] Sheng-Ye Zhang*[b] and Yan-Biao Kang *[a]

Visible-light irradiation with potassium *tert*-butoxide in dimethylformamide enables complete defluorination of sulfur hexafluoride under ambient conditions. Electron injection weakens the S–F bonds, producing intermediates that undergo stepwise cleavage. The process ultimately mineralizes SF_6 to sulfite and fluoride salts, demonstrating a low-energy strategy for activating extremely inert fluorinated molecules.

The global imperative to curb greenhouse gas emissions has renewed scrutiny of sulfur hexafluoride (SF_6), among the most potent and persistent anthropogenic climate forcers.[1] As a fully synthetic molecule with a highly symmetric octahedral geometry, in which six fluorine atoms are strongly bound to a central sulfur atom, SF_6 exhibits exceptional thermodynamic and kinetic stability. This inertness, together with its high electron affinity, enables efficient electron capture and suppression of electrical discharge, underpinning its widespread use in high-voltage power systems and electronics-related applications. However, these same physicochemical attributes render SF_6 uniquely problematic from an environmental perspective.[2] Its intense infrared absorption band at 915–960 cm^{-1} imparts a global warming potential approximately 23 500 times that of CO_2, while its atmospheric lifetime exceeds 3000 years.[3] Driven by continued industrial expansion, global SF_6 emissions surpassed 9000 metric tons in 2018,[4] and atmospheric concentrations rose beyond 12 parts per trillion (ppt) by 2025.[5] Collectively, these trends establish SF_6 as a critical target for international climate mitigation efforts and underscore the urgent need for effective degradation strategies.[6] Despite the urgent need to mitigate SF_6 emissions, activation of this exceptionally inert molecule remains intrinsically challenging. Existing industrial degradation processes rely on harsh conditions, including combustion[7] or high-temperature catalytic treatments[8,9] using metal phosphates or metal oxides, resulting in substantial energy consumption and the formation of toxic, highly corrosive decomposition products that necessitate complex operational protocols and stringent safety measures. Alternative strategies, such as reductive approaches,[10–15] nucleophilic activation,[16] and electrochemical methods, can cleave S–F bonds under comparatively milder conditions; however, these protocols often depend on hazardous reagents, expensive catalysts, or operationally complex procedures. Photochemical methods,[17] including ultraviolet-, laser-, and matrix-assisted activation, enable partial SF6 decomposition but typically require high-energy irradiation and rarely achieve complete mineralization.[18–25]

More recently, visible-light-mediated single-electron transfer processes[22,26–33] have enabled milder activation of SF_6; however, SF_6 is typically employed in large excess and serves primarily as an electron scavenger, restricting the reaction to partial reduction and precluding sequential S–F bond cleavage. These intrinsic limitations highlight the fundamental challenge of overcoming the extraordinary thermodynamic stability of SF_6 under low-energy irradiation while maintaining operational simplicity and avoiding toxic by-products. Consequently, the development of a mild and energy-efficient photoreductive pathway capable of complete SF_6 defluorination remains a significant challenge in sustainable fluorine-cycle management.

As part of our ongoing efforts to develop practical photochemical strategies for cleaving inert covalent bonds, we discovered that a combination of *N*,*N*-dimethylformamide (DMF) and potassium *tert*-butoxide (^{t}BuOK) under visible-light irradiation enables complete defluorination of the exceptionally inert greenhouse gas SF_6 under mild conditions (Fig. 1). This operationally simple process converts SF_6 quantitatively into non-toxic sulfite and fluoride salts, the latter of which can be repurposed as toothpaste additives, offering a practical and energy-efficient approach to sustainable fluorine-cycle management. Herein, we describe the implementation of this strategy and provide detailed mechanistic insights.

[a] *Department of Chemistry, University of Science and Technology of China, Hefei 230026, China. E-mail: ybkang@ustc.edu.cn*
[b] *State Key Laboratory of Organometallic Chemistry, Shanghai Institute of Organic Chemistry, Chinese Academy of Sciences, Shanghai, 200032, China. E-mail: zhangshengye@sioc.ac.cn*

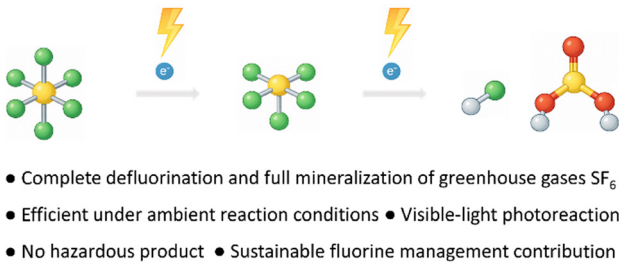

Fig. 1 Visible-light-mediated photoreductive defluorination of SF_6 in the presence of potassium *tert*-butoxide.

In an initial study, a sealed glass Schlenk flask charged with ^{t}BuOK and a magnetic stir bar was evacuated and backfilled with SF_6 and the selected solvent. As depicted in Fig. 2a and b, four blue LED beads were evenly mounted along the inner wall of an iron cylinder, with the reaction flask positioned at the centre of the chamber at an approximate distance of 3 cm from each LED to ensure uniform irradiation. Upon purple-light exposure, the reaction mixture underwent a gradual colour change, becoming light brown after 15 min and dark brown after 60 min. ^{19}F NMR spectroscopy revealed fluoride ions as the sole fluorine-containing species in the reaction mixture. Quantitative analysis using hexafluoro-2-propanol as an internal standard confirmed near-quantitative defluorination when DMF was used as the solvent.

Further mechanistic insight was obtained from atmospheric control experiments. The defluorination efficiency remained essentially unchanged under an inert nitrogen atmosphere, whereas performing the reaction in ambient air resulted in a pronounced decrease in conversion (Fig. 3a). This sensitivity to oxygen might result from the quenching of the photoexcited DMF-derived anion or other highly reducing, short-lived intermediates, underscoring their central role in SF_6 activation. Solvent effects were subsequently evaluated under otherwise identical conditions (Fig. 2c). Polar aprotic solvents, including DMF, NMP, and DMAc, afforded near-quantitative defluorination, whereas nonpolar or weakly coordinating solvents such as toluene and dioxane exhibited negligible activity. These observations indicate that solvent polarity and coordinating ability are critical for stabilizing reactive reducing species, thereby governing the efficiency of SF_6 activation.

The choice of base proved equally critical to reaction performance (Fig. 2d). Strong, sterically hindered alkoxides, most notably ^{t}BuOK, afforded the highest defluorination efficiency (up to 99%), whereas weaker bases or carbonate salts exhibited only marginal activity. Beyond intrinsic basicity, the identity of the counterion exerted a pronounced influence. Drapeau and co-workers, through combined NMR studies and computational analysis, demonstrated that alkali-metal cations stabilize the DMF anion and thereby facilitate deprotonation by *tert*-butoxide, whereas smaller cations such as Li^+ over-stabilize the anionic species, rendering its subsequent oxidation to the DMF radical kinetically unfavorable.[34] Consistent with this mechanistic framework, we observed a significant decrease in reaction rates in the presence of Na^+ and an even more pronounced suppression with Li^+ (Fig. 2d).

Systematic variation of ^{t}BuOK loading revealed a pronounced dose dependence, with increasing base concentration markedly accelerating the defluorination process (Fig. 2e). These results highlight the importance of balancing solvent polarity, base strength, and base concentration to achieve rapid and complete photoreductive defluorination. Time-course

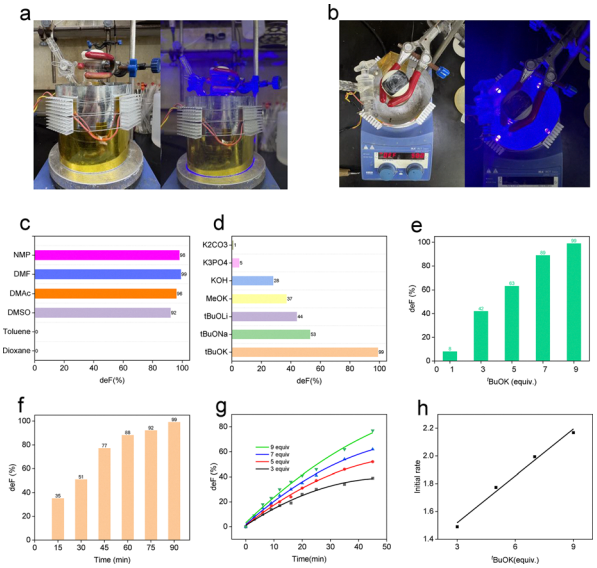

Fig. 2 (a) Side view of the reaction setup with light on (right) and off (left). (b) Top view of the reaction setup with light on (right) and off (left). (c) Effect of solvent on defluorination efficiency. (d) Effect of base on defluorination efficiency. (e) Effect of ^{t}BuOK loading on defluorination efficiency. (f) Effect of reaction time on defluorination efficiency. (g) Time-dependent fluoride formation under visible-light irradiation with varying ^{t}BuOK loadings (3, 5, 7 and 9 equiv.). (h) Initial rates extracted from the early linear regime, showing a near-linear dependence on ^{t}BuOK equivalents. Standard reaction conditions: SF_6 (29.2 mg, 0.2 mmol) and ^{t}BuOK (1.8 mmol, 9.0 equiv.) in 2.0 mL of DMF under the irradiation of 36 W LEDs (λ_{max} = 407 nm). Fluoride recovery yield was determined by ^{19}F NMR (in D_2O) analysis of the crude products using hexafluoroisopropanol as an internal standard.

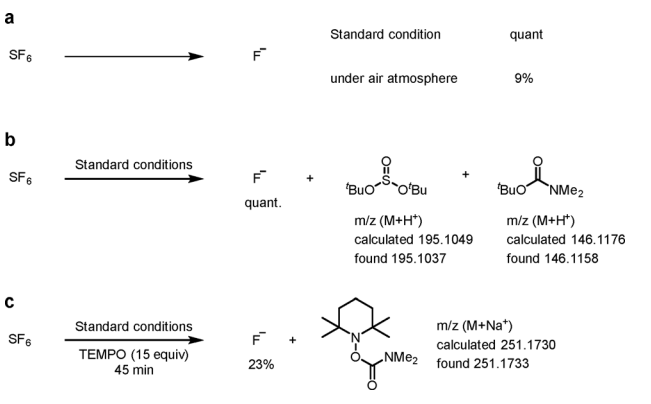

Fig. 3 (a) Influence of oxygen on the reaction. (b) Di-*tert*-butyl sulfite and *tert*-butyl dimethylcarbamate were detected by HRMS. (c) A deprotonated DMF radical was trapped using TEMPO.

analysis showed a rapid onset of reactivity, reaching 35% conversion within 15 min and near-quantitative defluorination (99%) after 90 min (Fig. 2f), consistent with an initially fast regime followed by gradual deceleration as reactive species are consumed. Kinetic analysis of the base dependence (Fig. 2g and h) revealed a first-order dependence of the initial rate on ^{t}BuOK concentration, indicating direct involvement of the base in the rate-determining step. Collectively, these findings suggest a dual role for ^{t}BuOK in the turnover-limiting elementary process: promoting the generation of highly reducing species and facilitating S–F bond cleavage. In concert with the solvent, ^{t}BuOK further stabilizes key intermediates, enabling efficient reaction progression until reagent depletion ultimately limits conversion.

With respect to sulfur-containing products, ion chromatography (IC) analysis of the crude reaction mixture identified KF, K_2SO_3 (S^{4+}) and K_2SO_4 (S^{6+}) as the major inorganic components. In parallel, high-resolution mass spectrometry (HRMS) of the reaction mixture revealed the formation of *tert*-butyl dimethylcarbamate and di-*tert*-butyl sulfite (Fig. 3b). To further clarify the identity and origin of the sulfur-containing species, the reaction mixture was subjected to distillation, and the resulting solid residues were analyzed by X-ray photoelectron spectroscopy (XPS), which confirmed K_2SO_3 and K_2SO_4 as the predominant sulfur-containing products. Taken together, these results indicate that K_2SO_3 arises from hydrolysis of di-*tert*-butyl sulfite formed *in situ*. Importantly, these findings demonstrate that SF_6 undergoes concurrent fragmentation and mineralization under the reaction conditions, thereby suppressing the formation of hazardous intermediates and underscoring the broad applicability of this method for end-of-life SF_6 remediation.

To evaluate scalability, an enlarged irradiation setup was constructed. Under these conditions, 99% defluorination was achieved within 3 h, demonstrating the robustness of the method and its potential for practical implementation in large-scale SF_6 remediation. Following the reaction, the solid inorganic salts were treated with BaF_2, and the resulting precipitate was removed by filtration. Analysis of the dried filtrate by ^{19}F NMR confirmed the presence of KF with high purity, demonstrating that the liberated fluoride could be efficiently recovered. This procedure afforded KF in 86% yield, highlighting both the operational practicality and material efficiency of the process (Fig. 4).

The decomposition of SF_6 is proposed to be initiated by electron injection, generating the radical anion $SF_6^{\bullet-}$, which rapidly fragments to yield a fluoride ion and the pentafluorosulfur anion (SF_5^-). In the first step, ^{t}BuOK deprotonates DMF to form the DMF anion (**Int1**). Although this deprotonation is endergonic, consistent with the relative acidities of ^{t}BuOH ($pK_a \approx 34$–35 in DMF) and DMF ($pK_a \approx 38$),[35,36] a small equilibrium concentration of the DMF anion is nonetheless expected (Fig. 5). Density functional theory (DFT) calculations by Alabugin and co-workers[37] indicate that deprotonation proceeds with a low enthalpic barrier ($\Delta H^{\ddagger}$ = 2.2 kcal mol^{-1}) and a transition-state Gibbs energy ($\Delta G^{\ddagger}$ = 12.6 kcal mol^{-1}) only slightly higher than that of the product, consistent with rapid

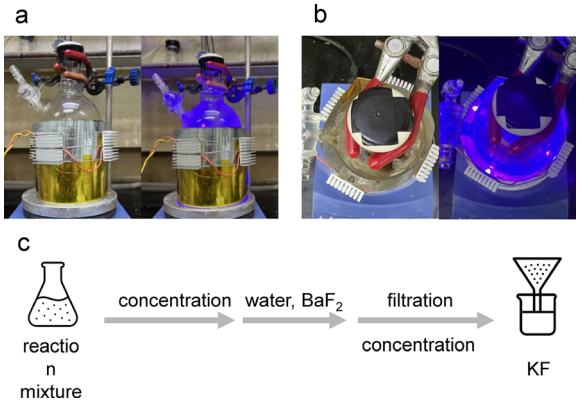

Fig. 4 (a) Side view of the gram-scale reaction setup under light irradiation (right) and without light irradiation (left). (b) Top view of the gram-scale reaction setup under light irradiation (right) and without light irradiation (left). (c) Recycling of KF obtained from the reaction.

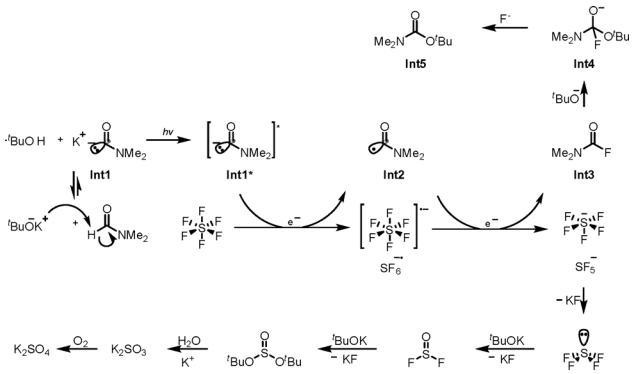

Fig. 5 Plausible mechanism.

and reversible proton transfer. Experimentally, the reaction is significantly slowed in the presence of Na^+ and, particularly, Li^+ (Fig. 2d), highlighting the critical role of basicity identity in modulating DMF anion formation.

Upon visible-light irradiation, the DMF anion (**Int1**) is photoexcited to a highly reducing state (**Int1***). Then the electron of **Int1*** can be transferred to SF_6, which concurrently yields $SF_6^{\bullet-}$ and the DMF radical (**Int2**). The DMF radical (**Int3**) then acts as a halogen-atom transfer (XAT) reagent, capturing a fluorine atom to form dimethylcarbamic fluoride (**Int4**) and SF_5^-.[38] In the presence of ^{t}BuOK, **Int4** is further converted to the corresponding fluorinated alkoxide species, ultimately yielding the neutral DMF derivative (**Int5**, Fig. 3b) and liberating a fluoride anion.

We performed DFT calculations at the theory level of PCM (DMF), ωb97xd/def2-TZVPP//PCM (DMF), and ωb97xd/def2-SVP with Gaussian 16 to elucidate the S–F bond cleavage and the roles of the solvent and base (Fig. 6). Photoexcitation of the anionic intermediate **Int1** and subsequent oxidation by SF_6 generate $SF_6^{\bullet-}$ and the radical **Int2**. Direct fluoride dissociation from $SF_6^{\bullet-}$ is thermodynamically unfavourable (ΔG = 21.8 kcal mol^{-1}). Instead, the radical **Int2** acts as a XAT mediator to facilitate

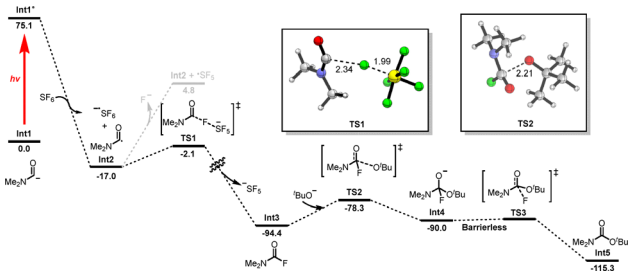

Fig. 6 DFT calculation.

capture of the fluorine atom. The XAT step exhibits a modest activation barrier ($\Delta G^{\ddagger}$ = 14.9 kcal mol^{-1}) and the formation of carbamic fluoride **Int3** is strongly exergonic (ΔG = −77.4 kcal mol^{-1}). Subsequent nucleophilic attack on **Int3** by ^{t}BuO^{-} then affords **Int4** ($\Delta G^{\ddagger}$ = 16.1 kcal mol^{-1}). Finally, **Int4** undergoes barrierless fluoride elimination (see Fig. S12) to yield the experimentally observed carbamate product **Int5**. The pentafluoro sulfide anion (SF_5^-) readily eliminates fluoride to form SF_4.[39] Under basic conditions, SF_4 reacts with ^{t}BuOK to yield di-*tert*-butyl sulfite, which is subsequently hydrolyzed to K_2SO_3.[40] K_2SO_4 can then be partially oxidized to K_2SO_4 during workup,[41] in agreement with the observed formation of both K_2SO_3 and K_2SO_4 in the reaction mixture.

In summary, we report a mild and efficient photoreductive strategy for the complete defluorination of SF_6 under ambient conditions. Visible-light irradiation in the presence of ^{t}BuOK and DMF generates transient carbonyl anions that mediate S–F bond cleavage, while the strongly basic environment enables sequential defluorination to form sulfite and fluoride salts. This operationally simple, waste-minimizing protocol provides a scalable approach for mitigating persistent SF_6 emissions and offers a practical route toward the sustainable management of legacy fluorinated greenhouse gases.

Conflicts of interest

The authors declare that they have filed a Chinese patent application (2026102165001) related to this work.

Data availability

The data underlying this study are available in the published article and its supplementary information (SI). Supplementary information: experimental details and NMR spectra for all compounds. See DOI: https://doi.org/10.1039/d6cc00483k.

Acknowledgements

We thank the Strategic Priority Research Program of the Chinese Academy of Sciences (XDA0540000) and the National Natural Science Foundation of China (22271268) for financial support. We acknowledge the Supercomputing Center of University of Science and Technology of China (USTC) for providing computational resources. The authors thank Dr Qiuhua Li at the University of Science and Technology of China (USTC) for helping with XPS characterization.

References

1 M. Maiss and C. A. M. Brenninkmeijer, *Environ. Sci. Technol.*, 1998, **32**, 3077–3086.
2 D. Edelson and K. B. McAfee, *J. Chem. Phys.*, 1951, **19**, 1311–1312.
3 A. R. Ravishankara, S. Solomon, A. A. Turnipseed and R. F. Warren, *Science*, 1993, **259**, 194–199.
4 N. Siddiqui, C. Weeks and J. Rogers, *IEEE Power Energy Mag.*, 2022, **20**, 132–138, DOI: 10.1109/MPE.2022.3153780.
5 NOAA Global Monitoring Laboratory. https://gml.noaa.gov/ccgg/trends_sf6/(accessed2025).
6 Z.-L. Cui, Y. Li, S. Xiao, S.-S. Tian, J. Tang, Y.-P. Hao and X.-X. Zhang, *Sci. Total Environ.*, 2024, **906**, 167347.
7 L. G. Christophorou, J. K. Olthoff and R. J. Van Brunt, *IEEE Electr. Insul. Mag.*, 1997, **13**, 20–24.
8 D. Kashiwagi, A. Takai, T. Takubo, K. Nagaoka, T. Inoue and Y. Takita, *Ind. Eng. Chem. Res.*, 2009, **48**, 632–640.
9 J. Zhang, J.-Z. Zhou, Q. Liu, G. Qian and Z.-P. Xu, *Environ. Sci. Technol.*, 2013, **47**, 6493–6499.
10 G. C. Demitras and A. G. MacDiarmid, *Inorg. Chem.*, 1964, **3**, 1198–1199.
11 H. L. Deubner and F. Kraus, *Inorganics*, 2017, **5**, 68.
12 D. K. Padma, V. Murthy, W. Becher and J. Massonne, *J. Fluorine Chem.*, 1973, **2**, 113–114.
13 G. Iakobson, M. Pošta and P. Beier, *J. Fluorine Chem.*, 2018, **213**, 51–55.
14 P. Holze, H. Bettina, L. Christian, M. Corinna and M. Stefan, *Angew. Chem., Int. Ed.*, 2014, **53**, 2750–2753.
15 L. Zámostná and T. Braun, *Angew. Chem., Int. Ed.*, 2015, **54**, 10652–10656.
16 F. Buß, C. Mück-Lichtenfeld, P. Mehlmann and F. Dielmann, *Angew. Chem., Int. Ed.*, 2018, **57**, 4951–4955.
17 D. Rombach and H.-A. Wagenknecht, *Synthesis*, 2022, 4883–4894.
18 L. Huang, Y. Shen, W. Dong, R. Zhang and H. Hou, *J. Hazard. Mater.*, 2008, **151**, 323–330.
19 D. Rombach and H.-A. Wagenknecht, *Angew. Chem., Int. Ed.*, 2020, **59**, 300–303.
20 S. Kim, Y. Khomutnyk, A. Bannykh and P. Nagorny, *Org. Lett.*, 2021, **23**, 190–194.
21 D. Rombach, B. Birenheide and H.-A. Wagenknecht, *Chem. – Eur. J.*, 2021, **27**, 8088–8093.
22 D. Rombach and H.-A. Wagenknecht, *ChemCatChem*, 2018, **10**, 2955–2961.
23 P. Rotering, C. Mück-Lichtenfeld and F. Dielmann, *Green Chem.*, 2022, **24**, 8054–8061.
24 Y. Yamada, H. Tamura and D. Takeda, *J. Chem. Phys.*, 2011, **134**, 104302.
25 (*a*) A. Sietmann, P. Heinzel, J. Gamper, D. Leitner, L. C. Pasqualini, F. R. S. Purtscher, H. Kopacka, T. S. Hoferm, A. Zemann and F. Dielmann, *Nat. Commun.*, 2026, **17**, 465; (*b*) J. Gao, D. Rao, Z. Liu, E. Yin, Z. Zhang, Q. Fu, M. Nogales and J. Liu, *Environ. Sci. Technol.*, 2025, **59**, 26865–26874.
26 T. A. McTeague and T. F. Jamison, *Angew. Chem., Int. Ed.*, 2016, **55**, 15072–15075.
27 A. Taponard, T. Jarrosson, L. Khrouz, M. Médebielle, J. Broggi and A. Tlili, *Angew. Chem., Int. Ed.*, 2022, **61**, e202204623.
28 C.-H. Jiang, H. Xu, Y.-G. Yang, M.-M. Zheng, Y. Zhao, Y.-W. Zuo, W.-R. Ren, S. Zhu, R.-X. Jin, X.-S. Xue and X.-S. Wang, *ChemRxiv.*, 2025, preprint, chemrxiv-2025-230kr, DOI: 10.26434/chemrxiv-2025-230kr.
29 X.-Y. Guo, S. Zhu, Y.-W. Zuo, Y. He, Y.-G. Yang, R.-X. Jin and X.-S. Wang, *Eur. J. Org. Chem.*, 2025, **28**(25), e202500314.
30 Z.-Y. Liu, Y. He, Y.-G. Yang, R.-X. Jin, S. Zhu and X.-S. Wang, *Org. Lett.*, 2025, **27**, 41–45.
31 Y.-F. Zhang, S. Zhu, Y.-W. Zuo, H. Liu, R.-X. Jin and X.-S. Wang, *Green Chem.*, 2024, **26**, 10324–10329.
32 Y.-W. Zuo, Y. Zhao, Y.-F. Zhang, X.-Y. Guo, T.-R. Wu, R.-X. Jin and X.-S. Wang, *Org. Lett.*, 2024, **26**, 5652–5656.
33 Y.-L. Huang, Q.-Q. Zhang, C.-Y. Wang, Y. Zhao and X.-S. Wang, *Org. Lett.*, 2024, **26**, 5776–5781.

34 M. Pichette Drapeau, I. Fabre, L. Grimaud, I. Ciofini, T. Ollevier and M. Tailefer, *Angew. Chem., Int. Ed.*, 2015, **54**, 10587–10591.
35 E. J. Nanni, M. D. Stallings and D. T. Sawyer, *J. Am. Chem. Soc.*, 1980, **102**, 4481–4485.
36 T.-H. Ding, J.-P. Qu and Y.-B. Kang, *Org. Lett.*, 2020, **22**, 3084–3088.
37 Q. Elliott, G. d P. Gomes, C. J. Evoniuk and I. V. Alabugin, *Chem. Sci.*, 2020, **11**, 6539–6546.
38 K. Matsumoto, Y. Haruki, S. Sawada, S. Yamada, T. Konno and R. Hagiwara, *Inorg. Chem.*, 2018, **57**, 14882–14889.
39 Y.-F. Chen, S.-Y. Gu, Y. Zhao, Y. You, F.-X. Ma, F. Zhu, S. Zhu and L.-G. Xie, *Green Chem.*, 2025, **27**, 2921–2930.
40 A. F. Janzen and R. K. Marat, *J. Fluorine Chem.*, 1988, **38**, 205–208.
41 M. Liu, *ACS Omega*, 2020, **5**, 13389–13395.